http://doi.org/10.35784/iapgos.6645 received: 30.09.2024 | revised: 20.10.2024 | accepted: 22.11.2024 | available online: 21.12.2024

IDENTIFICATION OF AN ARBITRARY SHAPE RIGID OBSTACLE ILLUMINATED BY FLAT ACOUSTIC WAVE USING NEAR FIELD DATA

Tomasz Rymarczyk[1,2], Jan Sikora[1,2]
[1]Research & Development Centre Netrix S.A., Lublin, Poland, [2]WSEI University, Faculty of Transport and Informatics, Lublin, Poland

Abstract. *The inverse problem concerning the identification of rigid surfaces of scattering objects formulated in the frequency domain is presented in this paper. Differences in the identification of concave objects, such as kite-shaped, and convex objects (circle) are indicated. The reader's attention is focused on the conventional boundary element method with small number of boundary elements and the small number of sensors, which is significant for inverse problems.*

Keywords: acoustics wave scattering by arbitrary shaped objects, simulation of external acoustic problems using the Boundary Element Method (BEM), inverse problem

IDENTYFIKACJA SZTYWNEJ PRZESZKODY O DOWOLNYM KSZTAŁCIE OŚWIETLONEJ PŁASKĄ FALĄ AKUSTYCZNĄ PRZY UŻYCIU DANYCH Z BLISKIEGO POLA

Streszczenie. *Zagadnienie odwrotne dotyczące identyfikacji sztywnych powierzchni obiektów rozpraszających sformułowanych w dziedzinie częstotliwości została przedstawiona w tej pracy. Wskazano na różnice w identyfikacji obiektów wklęsłych jak na przykład typu kite i wypukłych (okrąg). Skoncentrowano uwagę czytelnika na konwencjonalnej metodzie elementów brzegowych z oszczędną dyskretyzacją oraz ilością czujników pomiarowych co ma istotne znaczenia dla zagadnień odwrotnych.*

Słowa kluczowe: zagadnienie rozpraszania fal akustycznych przez obiekty o dowolnym kształcie, symulacja zewnętrznych zagadnień akustycznych Metodą Elementów Brzegowych (MEB), zagadnienie odwrotne

Introduction

Dealing with the acoustic scattering the frequency range is a critical issue.

Figure 1 shows how we understand the low, medium, and high frequency by means of the ratio between the acoustic wavelength $\boldsymbol{\lambda}$ and the characteristic geometrical dimension L of the arbitrary shaped scatterer (in Fig. 1 concave one).

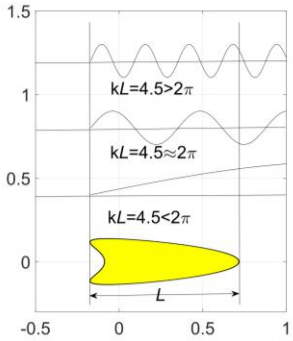

Fig. 1. Understanding of low medium, and high frequency range in terms of dimensionless wave number kL

The low frequency problem is when the acoustic wavelength. λ is significantly larger than the characteristic dimension $\lambda \gg L$ (see Fig. 1). The medium frequency range when λ is almost equal to L but high frequency range when wavelength λ is much smaller than the characteristic dimension $\lambda \ll L$.

Because in the title of the paper we have used an especially important term namely: "Near Field Data", a few words how we understand this term.

In general, in acoustic scattering problems, the distinction between the near field and the far field is crucial. Particularly especially when dealing with a rigid and concave scatterer as it will be shown in the subsequent subchapter.

The boundary between these two zones is conventional [5, 6] and depends on many factors, such as the dimensionless wavelength (kL where k is a wave number see for example Eq. 3) or the shape of the scatterer. In the near field, the shape of the scatterer has a significant impact on the acoustic field. There is a strong interaction between the sound waves and the scatterer's surface. This interaction can cause multiple reflections and diffractions which as we will see could cause some difficulties in the identification of the surface.

The near field is typically within a few wavelengths from the scatterer.

For the far field zone the acoustic field becomes more regular and predictable. The effects of the scatterer's shape diminish. Typically, the far field subregion is located at a greater distance from the scatterer, about several wavelengths away.

For a rigid and concave scatterer like the kite shaped one [8], the near field will exhibit due to the concavity more turbulent pattern. And this is the main problem of difficulties in scatterers shape reconstruction, what will be presented during the numerical experiments later.

1. The exterior forward problem of acoustic scattering

The problem is outlined by beginning with the time-harmonic reduction of the wave equation for the exterior forward problem to the Helmholtz equation [9, 10]:

$$\nabla^2\psi(\boldsymbol{r},t) = \frac{1}{c^2}\frac{\partial^2}{\partial t^2}\psi(\boldsymbol{r},t) \tag{1}$$

where: $\psi(\boldsymbol{r},t)$, [m^2/s] is the scalar time-dependent velocity potential related to the time-dependent particle velocity by relation $\mathbf{v}(\boldsymbol{r},t) = \nabla\psi(\boldsymbol{r},t)$ [m/s] (position vector $\boldsymbol{r}$, and t are the spatial and time variables in meters and seconds respectively) and c [m/s] is the propagation velocity.

Transferring from the time domain to the frequency domain the velocity potential ψ can be expressed as follows:

$$\psi(\boldsymbol{r},t) = \mathrm{Re}\{\varphi(\boldsymbol{r})\mathrm{e}^{-\mathrm{i}\omega t}\} \tag{2}$$

where: $\omega = 2\pi f$ [1/s] is the angular frequency, $\varphi(\boldsymbol{r})$ is the velocity potential amplitude and $i = \sqrt{-1}$ is the imaginary unit. The substitution of the above expression into the wave equation (1) reduces it to the Helmholtz equation of the form [4, 7]:

$$\nabla^2\varphi(\boldsymbol{r}) + k^2\varphi(\boldsymbol{r}) = Q \tag{3}$$

where: $k^2 = \frac{\omega^2}{c^2}$ and is the wavenumber and the wavelength is equal to $\lambda = c/f$, but the right-hand side Q stands for the acoustic source. The complex-valued function $\varphi(\boldsymbol{r})$ possess the magnitude and phase shift. The particle velocity has the similar form to the velocity potential see equation (2):

$$\mathbf{v}(\boldsymbol{r},t) = \mathrm{Re}\{\nabla\varphi(\boldsymbol{r})e^{-\mathrm{i}\omega t}\} \tag{4}$$

Often the normal component of the velocity on the boundary $\mathbf{v}_n(\boldsymbol{r})$ is imposed as a Neumann boundary condition:

$$\mathbf{v}_n(\boldsymbol{r}) = \nabla\varphi(\boldsymbol{r})\cdot\mathbf{n}_p = \frac{\partial\varphi(\boldsymbol{r})}{\partial n_p} \tag{5}$$

where $\mathbf{n}_\mathrm{p}$ is the unit outward normal to the boundary at point $\boldsymbol{r}$ [m] (see for example Fig. 2).

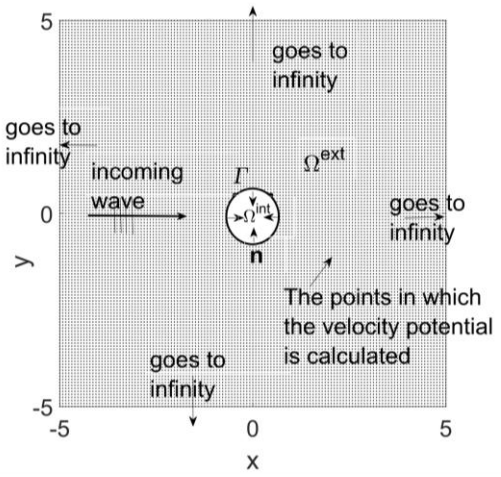

Fig. 2. External region under consideration illuminated by plane, time harmonic incident wave

The sound pressure p [1, 3] at the point $\boldsymbol{r}$ in the acoustic domain is one of the most useful acoustic properties, and it is related to the velocity potential $\varphi(\boldsymbol{r})$ by relation:

$$p(\boldsymbol{r}) = \mathrm{i}\omega\rho\varphi(\mathbf{r}) \left[\frac{1}{\mathrm{s}}\frac{\mathrm{kg}}{\mathrm{m}^3}\frac{\mathrm{m}^2}{\mathrm{s}} = \frac{\mathrm{kg}}{\mathrm{ms}^2} = \frac{\mathrm{N}}{\mathrm{m}^2} = \mathrm{Pa}\right] \quad (6)$$

In theoretical acoustics [10], it is often desirable to work with the Helmholtz equation (3) of the velocity potential φ instead of pressure p and/or vector of the particle velocity $\mathbf{v}$.

Considering above and making use of Green's second identity the Helmholtz equation (3) can be expressed in an equivalent form of a Boundary Integral Equation (BIE) [2, 13], i.e.:

$$c(\boldsymbol{r})\varphi(\boldsymbol{r}) + \int_{\boldsymbol{\Gamma}} \frac{\partial G(|\boldsymbol{r}-\boldsymbol{r}'|)}{\partial n}\varphi(\boldsymbol{r}')d\boldsymbol{\Gamma} = \\ = \int_{\boldsymbol{\Gamma}} G(|\boldsymbol{r}-\boldsymbol{r}'|)\frac{\partial\varphi(\boldsymbol{r}')}{\partial n}d\boldsymbol{\Gamma} + \varphi^{inc}(\boldsymbol{r}),\ \boldsymbol{r}\in\boldsymbol{\Gamma} \quad (7)$$

where φ^{inc} is the incident wave and the vector $\mathbf{n}$ is the unit normal vector outward pointing from the considered domain (see Fig. 2).

The coefficient $c(\boldsymbol{r})$ of Eq. (7) is equal to [9]:

$$c(\boldsymbol{r}) = \begin{cases} 0 & \text{if } \boldsymbol{r}\in\Omega^{\mathrm{int}}, \\ \frac{\text{angle}}{2\pi}(\text{in 2D}) & \text{subtended by exterior at } \boldsymbol{r} \text{ if } \boldsymbol{r}\in\boldsymbol{\Gamma}, \\ 1 & \text{if } \boldsymbol{r}\in\Omega^{\mathrm{ext}}. \end{cases} \quad (8)$$

As our interest is in the exterior problem, than $c(\boldsymbol{r}) = 1$.

The sound-hard scatterer is imposed through a homogeneous Neumann boundary condition $\left(\frac{\partial\varphi(\boldsymbol{r}')}{\partial n} = 0\right)$ on the boundary $\boldsymbol{\Gamma}$ (see Fig. 2). Making use of Green's second identity the Helmholtz equation can be expressed in an equivalent form of a Boundary Integral Equation (BIE) [7], i.e.

$$\varphi(\boldsymbol{r}) = -\int_{\boldsymbol{\Gamma}} \frac{\partial G(|\boldsymbol{r}-\boldsymbol{r}'|)}{\partial n}\varphi(\boldsymbol{r}')d\boldsymbol{\Gamma} + \varphi^{inc}(\boldsymbol{r}),\ \boldsymbol{r}\in\Omega^{\mathrm{ext}} \quad (9)$$

Due to the homogeneous Neumann boundary conditions the third term of Eq. (7) vanish. Now the boundary integral equation (9) for constant boundary elements can be written in terms of local coordinate ξ as follows [4]:

$$\varphi(\boldsymbol{r}) = -\sum_{j=1}^{M}\varphi_j(\boldsymbol{r}')\int_{-1}^{+1}\frac{\partial G(|\boldsymbol{r}-\boldsymbol{r}'|)}{\partial n}J(\xi)d\xi + \varphi^{inc}(\boldsymbol{r}) \quad (10)$$

where M – is the total number of constant elements, and $J(\xi)$ – is the Jacobian of transformation and is equal to, $J(\xi) = \frac{d\boldsymbol{\Gamma}}{d\xi} = \sqrt{\left(\frac{dx(\xi)}{d\xi}\right)^2 + \left(\frac{dy(\xi)}{d\xi}\right)^2} = \frac{L}{2}$, where L is the length of the constant boundary element [14].

If the plane wave is travelling along the unit vector $\mathbf{d}_0 = (\cos\theta_0, \sin\theta_0)$ (see Fig. 3) then $\varphi^{inc}(\boldsymbol{r}) = e^{ik(\boldsymbol{r}\cdot\mathbf{d}_0)}$, where the position vector $\boldsymbol{r} = |\boldsymbol{r}|e^{-i\theta}$ and $i = \sqrt{-1}$ is the imaginary unit.

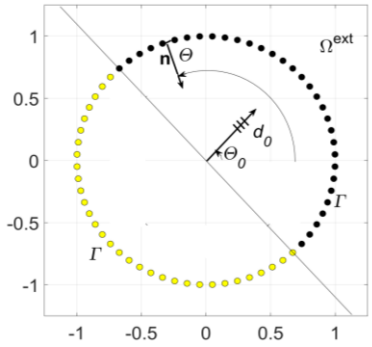

Fig. 3. Circular scatterer of radius R=1 and $\boldsymbol{d}_0$ direction vector of incoming wave. The yellow colour indicates illuminated part of boundary, but black colour shows the shaded side of the scatterer

So, the dot product $\boldsymbol{r}\cdot\mathbf{d}_0$ is, according to some mathematics, equal to $r_x\cos\theta_0 + r_y\sin\theta_0 = r\cos\theta\cos\theta_0 + r\sin\theta\sin\theta_0$ (see Fig. 3).

$$\varphi^{inc}(\boldsymbol{r}) = e^{ik(\boldsymbol{r}\cdot\mathbf{d}_0)} = e^{ik(r\cos\theta\cos\theta_0 + r\sin\theta\sin\theta_0)} = \\ = e^{ik(x\cos\theta_0 + y\sin\theta_0)} = \cos\big(k(x\cos\theta_0 + y\sin\theta_0)\big) + \\ + i\sin\big(k(x\cos\theta_0 + y\sin\theta_0)\big) \quad (11)$$

where: x and y are coordinates for which the velocity potential is calculated.

The Boundary Element solution (Fig. 4) will be compared with the analytical solution [12].

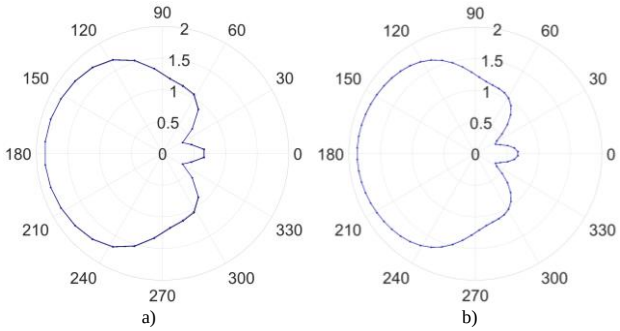

Fig. 4. Magnitude of the incoming and scattered wave on the perimetry of the circular scatterer a) for 32 boundary elements b) for 64 boundary elements

Based on analytical solution, easily achievable for circle only [12], the relative error would be calculated (see Fig. 5).

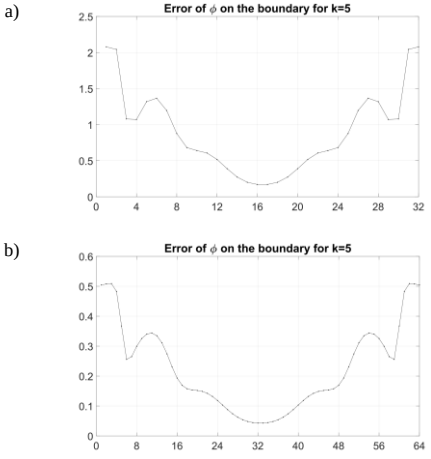

Fig. 5. Relative error [%] versus boundary element distribution along the circular scatterer boundary a) for 32 boundary elements b) for 64 boundary elements

Looking at the Fig. 4 we can conclude that the boundary element solution is almost identical with the analytical one. For thirty-two boundary elements the maximal relative error is 2.1% but for sixty-four boundary elements drop to 0.5%.

Our main interest is the Inverse Scattering Problem, so we are interested in as effective discretization as possible of the scatterer boundary. Considering all the restrictions mentioned by the Author in [9, 10], which were retained, for thirty-two boundary elements the maximum relative error was only 2,1% (Fig. 5) (on the shaded side of the scatterer). For the inverse problem, this should not be a problem. As we can observe in Fig. 5 on the most part of the boundary the relative error drop below 1%.

The scatterer is illuminated by the flat wave propagated with angle θ_0=0°. So, the wave is travelling from the left side to the right side of Fig. 6. In this case, as we are dealing with a convex figure having the analytical solution. Such a situation makes the comparison between numerical and analytical (see Fig. 6), but in contrary to the boundary solutions (Fig. 4 and Fig. 5), but not as easy.

In the subsequent figure (Fig. 6) we can observe the quantitative comparison between 3D visualization of the acoustic field around the scatterer achieved by the BEM solution and by the analytical one [12].

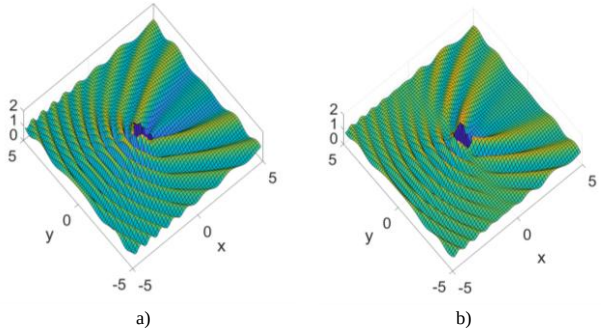

Fig. 6. Qualitative comparison of the relief plot for the scattering problem: a) BEM solution b) analytical solution

The circular scatterer is an excellent benchmark problem because it is easy to construct the analytical solution and, on this basis, it is possible to calculate the relative error for the boundary element solution. On this basis we have proved that software works correctly and, if we follow the acoustic advises [9, 10], it will be able to give correct results.

2. Concave scatterer

So far, we have considered only convex scatterers like circles. Now, it is time to deal with an arbitrary shaped scatterer. There are several types of such scatterers defined by a quite simple parametric equations [6, 15]:

$$x = a_v\cos(\theta) + b_v\cos(2 * \theta) + mvx$$
$$y = c_v\sin(\theta) + mvy, \qquad (12)$$

where: a_v, b_v, c_v and mvx, mvy are the coefficients responsible for the shape and position of the scatterer.

Some details about the parameters:

a_v is responsible for the size of the scatterer in x direction as well as the depth of concavity (inversely proportional); limits 0.1 – 1.0,

b_v= 0.1 – 1.0. This coefficient is also responsible for the depth of the concavity. The higher coefficient the deeper concavity.

c_v= 0.1 – 1.0 represent the height in y axis direction.

For differently shaped scatterers there are different parametric functions describing the shapes of the scatterers. Let us concentrate our attention on the kite like scatterer defined by Eq. (12).

Using one simple parametric functions Eq. (12) we can generate different shapes of the region. Such a description might be particularly useful in the tomography problems solved by BEM.

In the Figure 7 are presented different angles of the incoming flat wave for the kite scatterer. Also, we can observe how the concave scatterer's boundary is illuminated.

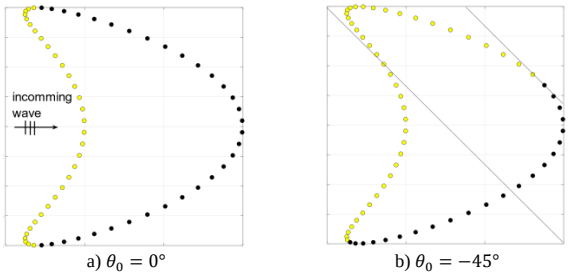

Fig. 7. Single kite scattering object: a) incoming flat wave from left to right side with illuminated (yellow) and shadowed side (black) of the boundary, b) incoming wave from upper left corner to lower right corner of the kite scatterer with illuminated and shadowed boundaries marked by yellow and black colour respectively

Using the boundary element technique, it is quite easy to calculate the shadow or the illuminated boundary zones. The zone consists of collection of boundary elements and could be calculated in the following way:

$$\boldsymbol{n_j} \cdot \mathbf{d} > \mathbf{0}$$

where the plane wave is travelling along the unit vector $\mathbf{d} = (\cos\theta_0, \sin\theta_0)$ and $\boldsymbol{n_j}$ is the unit normal vector of j^{th} boundary element, directed outside the investigated region. So, the dot product $\boldsymbol{n_j} \cdot \mathbf{d}$ after some mathematics the dot product is equal to $n_{jx}\cos\theta + n_{jy}\sin\theta = \cos\theta_j\cos\theta_0 + \sin\theta_j\sin\theta$ (see Fig. 3). The angle of θ_j is the angle of the position vector of boundary element which in this case (circle) means that it is an angle of the normal outside vector of the boundary element.

3. Numerical experiments with the concave scatterer

The numerical experiment was reduced to an optimisation task [11] where, at each iterative step, sensor measurements were compared with the measurement results for the so-called real object. Since the forward problem was formulated in the frequency domain, the objective function must be defined as the product of the difference of the measurement signals (complex numbers) by their complex conjugate value [14], thus obtaining a scalar quantity.

The measurement data is taken at 8 or 16, for higher frequency range, uniformly distributed points on the boundary $\boldsymbol{\Gamma}$ (see Fig. 8 and Fig. 9), whose values are obtained by solving the corresponding forward scattering problem Eq. (10), using the standard boundary integral equation method with only 32 grid points on the boundary $\partial\boldsymbol{\Gamma}$.

White noise is added to the data as $u_\delta(R_\Gamma, \theta_j) = u_\delta(R_\Gamma, \theta_j)(1 + \delta N_j)$, where N_j are values sampled from the standard normal distribution of physical units, namely velocity potential [m^2/sec] at each boundary element. Let the noise level $\delta = 10\%$ be fixed for all numerical experiments.

In this section we would like to present some numerical examples to show some results of this approach and the dependence of the results on various parameters. The experiment is carried out for two different frequency ranges: the low range and the high range which is quite close to the medium range. The measurement data are taken at the boundary $\boldsymbol{\Gamma}$ in points where the acoustic sensors have been fixed (see Fig. 8).

Looking at the results from Fig. 8, we see that not all the illumination angles provide satisfactory results, even for the angles of incidence of the plane wave, which should be straightforward, e.g., -π/2 and 0. The optimisation finds a local minimum, from which it is difficult to escape (see Fig. 8c and Fig. 8f).

We conducted a similar experiment for high frequency. This time, with only eight sensors, it was not possible to obtain any satisfactory results. Doubling the number of sensors resulted in a radical improvement. However, compared to the previous experiment, the results were far from satisfactory in some cases (for example Fig. 9a-c).

The Fig. 10 shows the image of the total field in the near field and its equipotential lines.

To illustrate how difficult is the shape identification for a concave scatterer, we conducted a numerical experiment for a circle (Fig. 11a) and for a kite-shaped scatterer (Fig. 11b), maintaining identical conditions except, of course, for the shape of the scatterers. This experiment was conducted for the high frequency range. Even though the circuit produced the correct results for the 10% noise kite like scatterer failed.

The results speak for themselves.

$kL \approx 2.5 \cdot 0.5 = 1.25 << 2\pi$ low frequency range (L – characteristic dimension of the scatterer).

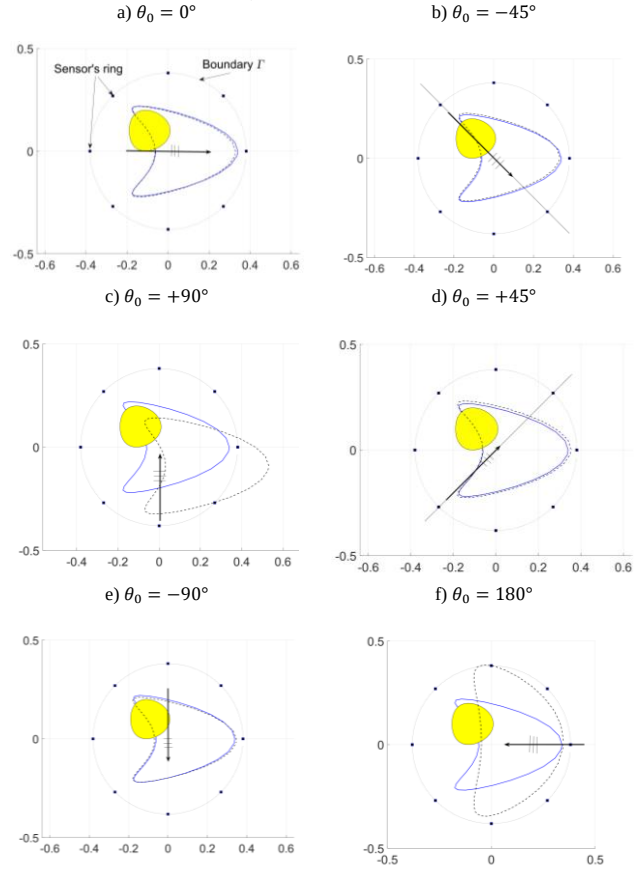

a) $\theta_0 = 0°$ b) $\theta_0 = -45°$ c) $\theta_0 = +90°$ d) $\theta_0 = +45°$ e) $\theta_0 = -90°$ f) $\theta_0 = 180°$

Fig. 8. Low frequency range results of the optimisation: the yellow object means the starting point of the optimisation, the blue solid line represents the real scatterer but the dashed black line is the final results of the optimisation

$kL \approx 5 \cdot 1.7 = 8.5 \gg 2\pi$ high frequency range but with a tendency to the mid-range.

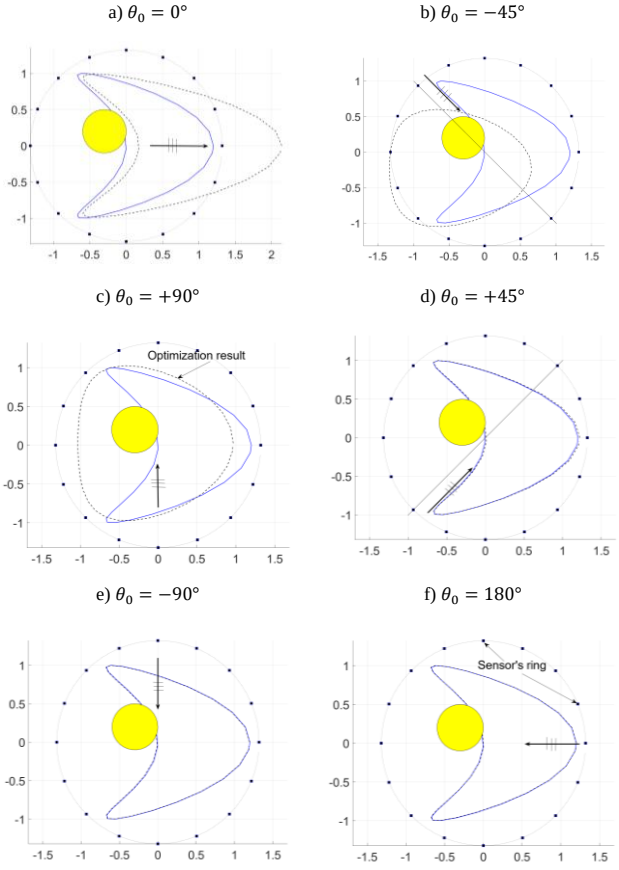

a) $\theta_0 = 0°$ b) $\theta_0 = -45°$ c) $\theta_0 = +90°$ d) $\theta_0 = +45°$ e) $\theta_0 = -90°$ f) $\theta_0 = 180°$

Fig. 9. Results of optimisation:the yellow object is the starting point of optimisation, the blue solid line represents the real scatterer but the dashed black line is the final result of optimisation

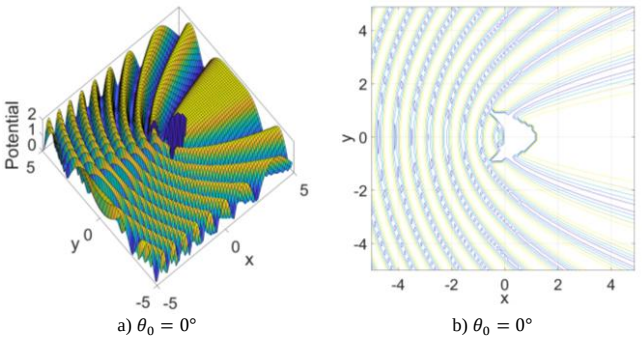

a) $\theta_0 = 0°$ b) $\theta_0 = 0°$

Fig. 10. Results of the optimisation for the absolute complex velocity potential and its equipotential lines

$kL \approx 15 \cdot 0.5 = 7.5 \gg 2\pi$

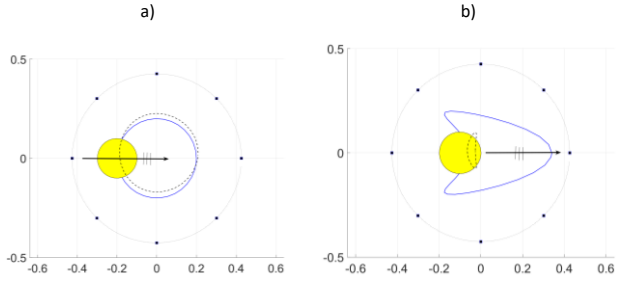

Fig. 11. Convex versus concave optimisation

4. Conclusions

Concluding the results of numerical experiments, we can say that the deterministic optimisation method for identification of the shape of the rigid surface of the scatterer is working well when for the concave scatterer not really. We can see that for different angles of illumination of the scatterers by the flat wave the results are quite different. This is a numerical modelling, so we must deal with many local minima, and keeping in mind that the sensitivity analysis is made by the numerical approach, and it is difficult to achieve a fully satisfactory result.

The authors suggest two ways of solving these difficulties. First it is worth to try an optimisation procedure which could give a chance to find out the global minima. And the natural choice is a Genetic Algorithm [15]. But also, we can change a little a definition of the problem itself. Here it would be helpful to use, for example, the idea of Electrical Impedance or Diffuse Optical Tomography [14].

According to this concept, the scatterer can be sequentially illuminated from different angles, which are called projection angles. And for such a model, a deterministic optimisation method might give much better results.

References

[1] Abramowitz M., Stegun I. A.: Handbook of mathematical functions with formulas, graphs, and mathematical tables. John Wiley, New York 1973.
[2] Akylas T. R., Mei C. C.: I-campus project School-wide Program on Fluid Mechanics Modules on Waves in fluids. Chapter Five of Reflection, Transmission and Diffraction [http://web.mit.edu/fluids-modules/waves/www/c-index.html].
[3] Baynes A. B.: Scattering of low-frequency sound by compact objects in underwater waveguides. PhD Dissertation. Naval Postgraduate School, Monterey, California 2018.
[4] Becker A. A.: The boundary Element Method in Engineering. A complete course. McGraw-Hill Book Company 1992.
[5] Cakoni F., Colton D.: A Qualitative Approach to Inverse Scattering Theory. Applied Mathematical Sciences 188. Springer 2014.
[6] Colton D., Kress R.: Integral Equation Methods in Scattering Theory. Springer 1993.
[7] Jabłoński P.: Engineering Physics – Electromagnetism. Częstochowa University of Technology 2009.
[8] Jeong C., Na S.-W., Kallivokas L. F.: Near-surface localization and shape identification of a scatterer embedded in a halfplane using scalar waves. Journal of Computational Acoustics 17(3), 2009, 277–308.
[9] Kirkup S., The Boundary Element Method in Acoustics: A Survey. Applied Sciences 9(8), 2019, 1642 [https://doi.org/10.3390/app9081642].
[10] Kirkup S.: The Boundary Element Method in Acoustics. Book in Journal of Computational Acoustics 2007.
[11] Li P., Wang Y.: Numerical solution of an inverse obstacle scattering problem with near-field data. Journal of Computational Physics 290, 2015, 157–168.
[12] Lynott G. M.: Efficient numerical evaluation of the scattering of acoustic and elastic waves by arrays of cylinders of arbitrary cross section. Thesis of Doctor of Philosophy. University of Manchester, School of Natural Sciences, Department of Mathematics, 2020.
[13] Rymarczyk T.: Tomographic Imaging in Environmental, Industrial and Medical Applications. Innovatio Press Publishing Hause, Lublin 2019.
[14] Sikora J.: Boundary Element Method for Impedance and Optical Tomography. Warsaw University of Technology Publishing Hause, Warsaw 2007.
[15] https://www.mathworks.com/products/matlab.html

D.Sc. Ph.D. Eng. Tomasz Rymarczyk
e-mail: tomasz@rymarczyk.com

He is the director in Research and Development Centre in Netrix S.A. and the director of the Institute of Computer Science and Innovative Technologies in the University of Economics and Innovation, Lublin, Poland. He worked in many companies and institutes developing innovative projects and managing teams of employees.
His research area focuses on the application of non-invasive imaging techniques, electrical tomography, image reconstruction, numerical modelling, image processing and analysis, process tomography, software engineering, knowledge engineering, artificial intelligence, and computer measurement systems.

http://orcid.org/0000-0002-3524-9151

Prof. D.Sc. Ph.D. Eng. Jan Sikora
e-mail: sik59@wp.pl

Prof. Jan Sikora (Ph.D. D.Sc. Eng.) graduated from Warsaw University of Technology Faculty of Electrical Engineering. During 44 years of professional work, he has obtained all grades, including the position of full professor at his alma mater. Since 1998 he has also worked for the Institute of Electrical Engineering in Warsaw. In 2008, he has joined Electrical Engineering and Computer Science Faculty in Lublin University of Technology. During 2001-2004 he has worked as a Senior Research Fellow at University College London in the prof. S. Arridge's Group of Optical Tomography. His research interests are focused on numerical analysis application in the field theory. He is an author of eight books and more than 180 papers published in the international journals and conferences.

http://orcid.org/0000-0002-9492-5818